Neuromorphic Decoding of Spinal Motor Neuron Behaviour during Natural Hand Movements for a New Generation of Wearable Neural Interfaces

Simone Tanzarella (s.tanzarella17@imperial.ac.uk)
https://orcid.org/0000-0003-0960-6562

Massimiliano Iacono
Istituto Italiano di Tecnologia

Elisa Donati
Eidgenossische Technische Hochschule Zurich

Dario Farina
Imperial College London

Chiara Bartolozzi
Istituto Italiano di Tecnologia https://orcid.org/0000-0003-3465-6449

Research Article

Keywords: Neural interfaces, Spinal Motor Neurons, Spiking Neural Networks, Neuromorphic, Wearable

Posted Date: March 18th, 2022

DOI: https://doi.org/10.21203/rs.3.rs-1465054/v1

Neuromorphic Decoding of Spinal Motor Neuron Behaviour during Natural Hand Movements for a New Generation of Wearable Neural Interfaces

Simone Tanzarella[1,2*], Massimiliano Iacono[2], Elisa Donati[2,3], Dario Farina+[1] and Chiara Bartolozzi+ [2]

[1]Department of Bioengineering, Imperial College London, Exhibition Road, SW7 2AZ, UK.
[2*]Event-Driven Perception for Robotics Department, Istituto Italiano di Tecnologia, Via San Quirico 19D, Genova, 16163, Italy.
[3]Institute of Neuroinformatics, ETH Zurich, Winterthurstrasse 190, 8057, Switzerland.

*Corresponding author(s). E-mail(s): s.tanzarella17@ic.ac.uk;
Contributing authors: massimiliano.iacono@iit.it; elisa@ini.uzh.ch; dario.farina@imperial.ac.uk; chiara.bartolozzi@iit.it;

Abstract

We propose a neuromorphic framework to process the activity of human spinal motor neurons for movement intention recognition. This framework is integrated in a non-invasive interface that decodes the activity of motor neurons innervating intrinsic and extrinsic hand muscles. One of the main limitations of current neural interfaces is that machine learning models cannot exploit the efficiency of the spike encoding operated by the nervous system. Spiking-based pattern recognition would detect the spatio-temporal sparse activity of a neuronal pool and lead to adaptive and compact implementations, eventually running locally in embedded systems. Emergent Spiking Neural Networks (SNN) have not yet been used for processing the activity of in-vivo human neurons. Here we developed a convolutional SNN to process a total of 467 spinal motor neurons whose activity was identified in 5 participants while

*+Dario Farina and Chiara Bartolozzi share the senior authorship.

executing 10 hand movements. The classification accuracy approached **0.95 ± 0.14** for both isometric and non-isometric contractions. These results show for the first time the potential of highly accurate motion intent detection by combining non-invasive neural interfaces and SNN.

Keywords: Neural interfaces, Spinal Motor Neurons, Spiking Neural Networks, Neuromorphic, Wearable

1 Introduction

Next generation of Human Machine Interfaces (HMIs) aims at fast, safe, touchless and intuitive control of digital devices, based on the prediction of human intention obtained by decoding neural activity, through neural interfaces. Applications range from the control of smart devices (smartphones, home, virtual and augmented reality), to the control of assistive devices and robots.

Neural interfaces extract information from different regions of the nervous system and differ in the degree of their invasiveness. Implanted electrodes directly measure the activity of neurons (e.g., electroneuronography (ENG), electrocorticography (ECoG), Microelectrode arrays (MEAs)), while non-invasive measures (Electroencephalography (EEG), surface electromyography (sEMG), etc.) provide a global information on neural activity [1, 2]. Motor intent can also be decoded from recordings from muscle tissue, e.g. myoelectric control of prosthetic limbs [3–6]. The Electromyography (EMG) signal is generated by the neural activity of the spinal motor neurons that innervate the recorded muscles and therefore it embeds the neural drive sent from the spinal cord to muscle. Accordingly, it has been proven that the discharge times of spinal motor neurons can be exactly identified by processing intramuscular or surface (non-invasive) EMG signals. Accessing single motor neuron activity from the sEMG has been shown to be an effective way to extract movement intentions for controlling external devices [7]. By identifying the activity of single motor neurons from the EMG, the information sent by the Central Nervous System (CNS) to activate muscles is decoupled from the muscle fibres action potentials, de-facto accessing information about the CNS through the muscular system [7–12].

When establishing a neural interface by decoding muscle electrical signals, the extracted spiking activity of neurons is usually transformed into non-spiking features, moving from a binary discrete domain to a continuous one, or using a set of kernels to extract a richer information from spike trains in terms of neural recruitment strategies, such as identification of neurons encoding for a specific function, spike train similarity, and probability distribution of spiking neuronal behaviour [13]. Spiking Neural Network (SNN)-based machine learning, however, would address the full information potential of the intrinsic spiking nature of motor neuron firing patterns, exploiting the complexity

of their spatio-temporal sparse activity and leading to adaptive and extremely efficient and compact implementations on neuromorphic hardware. Information in neural systems is encoded at population level (spatial) in the precise temporal pattern of spikes, as demonstrated in somatosensory [14, 15] and visual and audio [16] cortex for sensory stimuli and decision making [17]. Thus, we here hypothesise that SNN-based architectures have the potential to efficiently decode the sparse activity of a large number of motor neurons involved in the generation of complex hand motion patterns across different tasks.

Neural and synaptic models implemented in SNNs can replicate the spiking and local learning functions of real neurons [18]. These models are closer to the underlying physiology than those used in classic deep learning [19], and can be successfully implemented in Very Large Scale Integration (VLSI) neuromorphic circuits [20, 21]. Neuromorphic hardware asynchronously executes the operations of the neurons in the implemented networks and substantially reduces the computational cost, processing time, latency, and energy consumption [22, 23]. Although implementations of SNNs on neuromorphic hardware are currently limited to basic proofs-of-concept, they show promising results in terms of latency and power consumption, especially for biomedical signal processing [24–28]. Despite their intrinsic spiking nature, only few attempts have been proposed to process spiking information from biological neurons, either from in-vitro neuronal cultures obtained by animal cortical tissues [29–31] or in-vivo from anesthetized animals [32].

In this study, we show for the first time the processing of human in-vivo spiking activity of individual spinal motor neurons with a SNN during the execution of daily-life gestures. With this approach, we show the detection of natural finger movements from pools of motor neurons innervating 14 hand muscles. The classification of finger movements was performed by a convolutional SNN based on surrogate gradient descent and local learning [33]. We explored a user-centred approach, by implementing user-specific hyperparameter tuning, and we attempted to solve the problem of the variability in the number of identified motor neurons across different subjects and different sessions for the same subject. The proposed SNN-based architecture provides the basis for the development of non-invasive, wearable neural interfaces for the next generation of intuitive HMIs for a broad range of daily-life conditions, such as touchless control of devices, gaming and controlling virtual reality, as well as for control of prostheses and rehabilitation.

2 Results

2.1 Human neural spiking activity processed with spiking neural networks

The spiking activity of individual spinal motor neurons innervating muscles in the hand (intrinsic) and in the forearm (extrinsic) actuating fingers and wrist was directly interfaced with a convolutional SNN composed by two layers

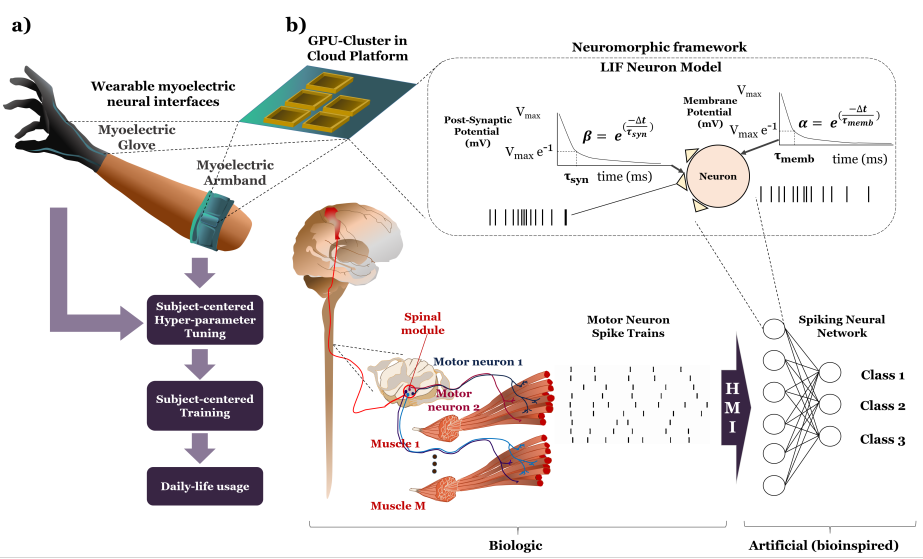

Fig. 1 Non-invasive neural interfaces for neuromorphic implementation. Human spinal motor neurons spike trains, inferred from surface electromyography (sEMG), are interfaced with an artificial Spiking Neural Network (SNN) of Leaky Integrate-and-Fire (LIF) neurons with local learning rules. The input to motor neurons is the net output of the integration performed by spinal interneurons of supraspinal and afferent neurons, encoded in the spiking activity of the motor neuron. The SNN main hyperparameters are α and β, the neuron's membrane and synaptic time constants, respectively.

of LIF neurons (Fig. 1) to identify the performed hand gesture. Decomposition extracts spiking information of single motor neurons non-invasively from High-Density-sEMG (HD-sEMG) signals. It consists in separating the firing occurrences from the motor unit action potential waveforms (Fig. 2.b). These waveforms do not correspond to neural information and depend only on the volume conduction, i.e. properties of the recording system, interposed tissues and the relative distance between active motor units and electrodes [34]. Each identified waveform for a motor unit corresponds to a spike in the innervation pulse train and the relative firing occurrences are extracted by thresholding. The output of the decomposition is a collection of time-varying inter-pulse trains (IPTs), the sequence of firing occurrences for each identified motor unit (Fig. 2.b). The spiking information of single motor neurons is the net product of the integration at the spinal level between the central supraspinal commands and the peripheral afferent commands performed by modules of interneurons. The number of recruited motor neurons and their firing rate determine the overall control signal to modulate muscle force exertion.

To record the HD-sEMG dataset, we asked the subjects to perform different types of gestures by flexing each individual finger in three different wrist postures – neutral, flexed and extended – and also thumb abduction and opposition, since these degrees of freedom of the thumb are involved in grips and object manipulation. For the same reason we asked to simulate three different

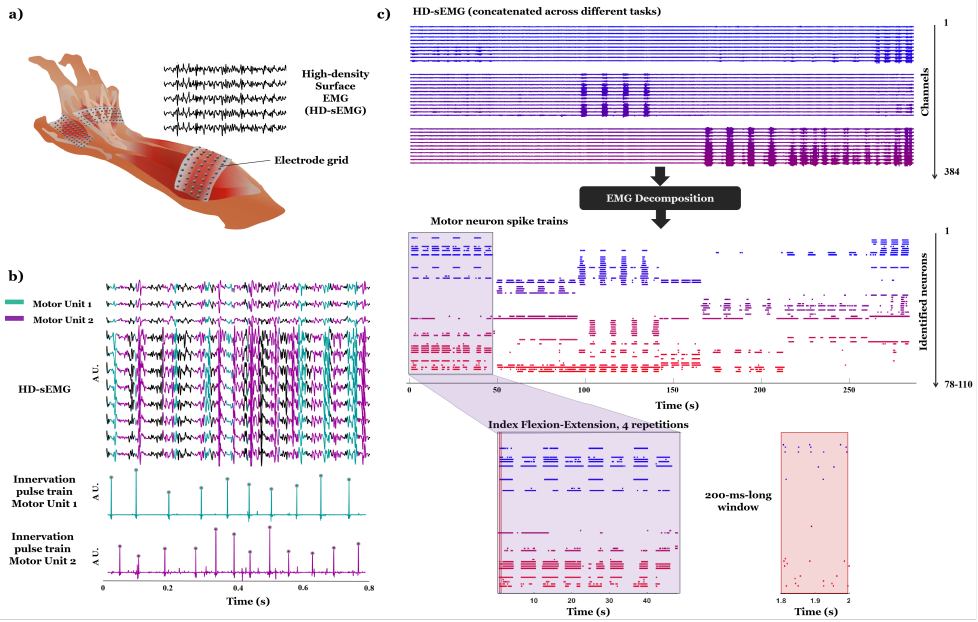

Fig. 2 Signal processing and motor neuron identification. a) High-Density-sEMG (HD-sEMG) recordings, concatenated across tasks, are decomposed in the corresponding trains of motor unit action potentials, to obtain the relative motor neuron spike trains tracked across different tasks. b) Identification of 2 motor units by HD-sEMG decomposition: the decomposition exploits blind source separation to distinguish similar motor unit action potential waveforms. c) The identified spike trains for one task are segmented in 200 ms-width windows and used as inputs to the convolutional Spiking Neural Network (SNN).

grips, without contact with objects, i.e. two-finger, three-finger and five-finger grips. These 10 natural gestures, which we considered the same across different wrist posture, are represented in Fig. 3.a.

The number of identified motor neurons analysed in this study is reported in Table 1. Their activity was tracked across all the 10 tasks (as shown in Fig. 2.c) for each of the 5 subjects. On average, 93.4 ± 13.8 motor neurons per subject were identified (467 in total) and the accuracy of this identification was quantified by a pulse-to-noise ratio (PNR) [35] equal to $32.2 \pm 5.0 dB$ across all motor neurons. As explained in [35], this value of the PNR corresponded to an average decomposition accuracy of $> 90\%$ (see Section 4). The identified motor neurons for all subjects, across all their activities, presented a mean firing rate of 13.2 ± 7.9 Hz. In the table, motor neurons are grouped by the 14 targeted muscles represented in Figure 3.b and covered by 64-channels HD-sEMG electrode grids placed as explained in detail in [36]. More than ten of the most important muscles actuating the finger and the wrist were targeted, both to map more completely the biomechanic of hand movements and to simulate the usage of a high-density myoelectric glove for intrinsic muscles or a more traditional high-density myoelectric band around the forearm, over extrinsic muscles.

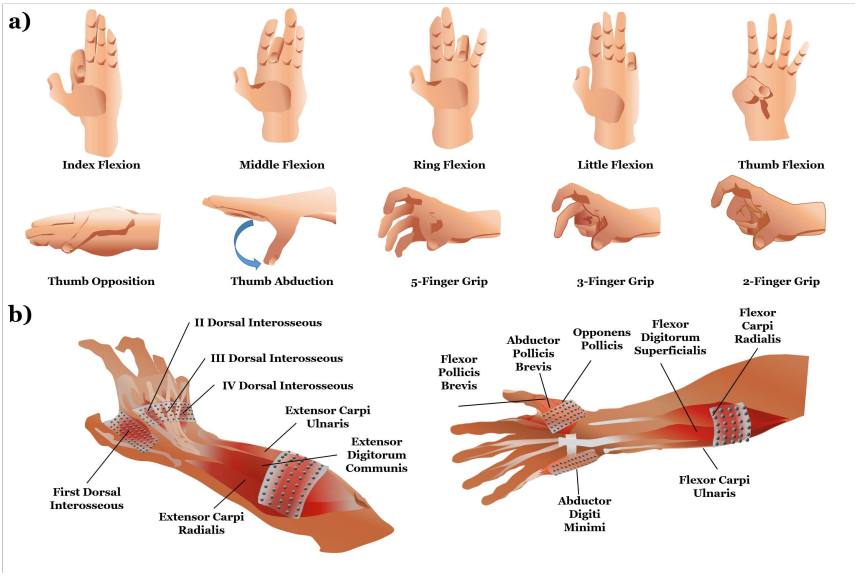

Fig. 3 Experimental protocol and High-Density-sEMG (HD-sEMG) electrode placement. a) The protocol included single-finger flexion (5 gestures), 3 different grips with 5, 3 and 2 fingers, and thumb abduction and opposition (10 gestures in total). b) 6 HD-sEMG grids each with 64-channels recorded the activity of 14 muscles. Two large grids (8mm Intra-Electrode Distance (IED)) were placed over the forearm and four small grids were placed over intrinsic muscles (4mm IED).

Different parts of the dataset were separately classified: increasing (I), plateau contractions (P), and both together (I+P), obtained by segmenting each repetition for each task in the corresponding 2 s-long phases. Two different sets of classes were tested: 5 classes (with only the single-finger flexion), and 10 classes, adding the 3 grips and the 2 thumb opposition gestures.

2.2 Optimal hyperparameters

The proposed convolutional SNN is based on the Deep Continuous Local Learning (DECOLLE) framework [33] (Fig. 4.b). The hyperparameters which have the greatest impact on the performance are the dimension of the input window, the number and size of the layers and the time constants of neurons and synapses.

The spike trains of all the considered motor neurons of all muscles for each subject, windowed at 200 ms, were sent to the 1-D input array of the network. We chose the minimum number of layers (two) in the convolutional architecture (Fig. 4.a), to optimise the trade-off between accuracy and power consumption. The first convolutional layer has an input size equal to the number of the processed motor neurons, that is different for each subject (Table 1), and an output of 64 (set empirically after preliminary tests); the second has an input of 64 and an output of 128. Each layer is trained locally, using the classification of the gestures in a fully connected readout layer as objective function. Each

Table 1 Number of identified motor neurons for each muscle for the 5 subjects.

	Subjects				
Muscle	S1	S2	S3	S4	S5
FDI	10	17	20	11	19
IIDI	5	6	9	3	8
IIIDI	7	7	7	5	7
IVDI	7	3	4	6	6
ADM	7	12	9	14	8
FPB	0	2	0	0	3
APB	0	4	11	6	3
OPP	3	9	6	7	14
ECU	9	6	4	4	7
EDC	8	6	9	5	9
ECR	6	4	5	0	4
FCU	6	8	8	6	6
FDS	10	11	11	11	12
FCR	3	0	0	0	4
Tot Intr	39	60	66	52	68
Tot Extr	42	35	37	26	42
Total	81	95	103	78	110

of these readout layers produced a number of outputs equal to the number of classes to discriminate. Further details are provided in Section 4.

The time constants of the synapses τ_{syn} and membrane potential τ_{mem} of the LIF neurons are encoded in the $\alpha = e^{\frac{-\delta t}{\tau_{mem}}}$ and $\beta = e^{\frac{-\delta t}{\tau_{syn}}}$ hyperparameters. They were tuned for each subject separately by testing the network on all the 10 classes, by considering the contraction phase I+P and a window width of 200 ms with no overlap. This hyperparameter tuning was run on 40 % of the

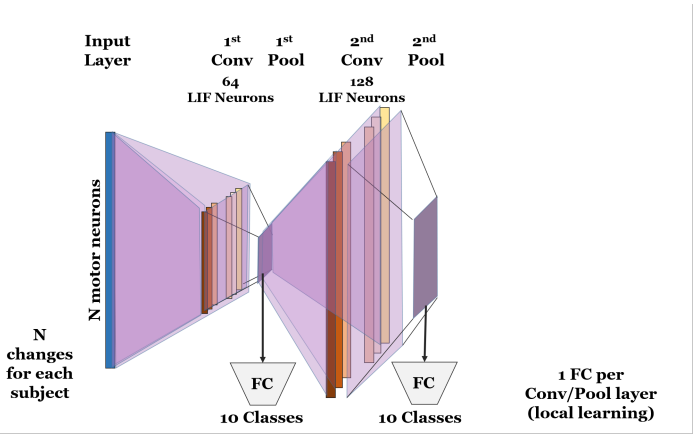

Fig. 4 Structure of the convolutional Spiking Neural Network (SNN) adopted in the study. The overall structure of the network comprises two convolutional spiking layers (Conv), and two pool layers (Pool). Two fully connected (FC) layers are appended each one at the end of each Conv-Pool structure, to implement the local learning. The dimension of their output is the number of classes. The number of neurons (N) in the input layer corresponds to the number of motor neurons identified for each subject, varying for each subject, as reported in Table 1.

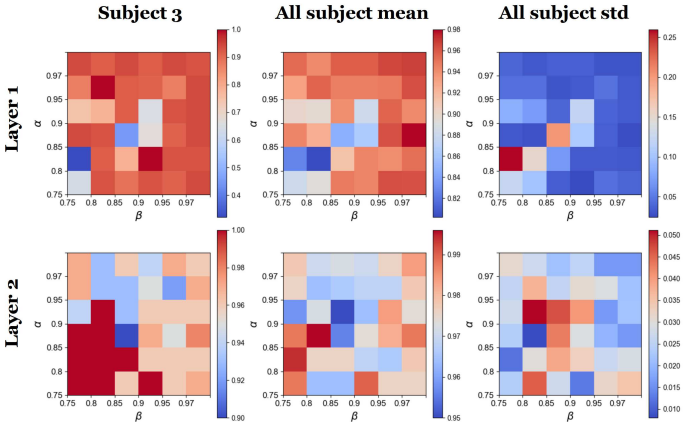

Fig. 5 Grid search for the optimisation of the hyperparameters α and β, respectively related to the membrane and synaptic constants. Mean and standard deviation across subjects and network layers of the maximal test accuracy across 100 epochs of training are reported, normalised between 0 and 1.

Table 2 Chosen values of α and β for the 5 subjects.

	Subjects				
	S1	S2	S3	S4	S5
α	0.80	0.97	0.80	0.75	0.97
β	0.75	0.95	0.90	0.95	0.90

available dataset. The remaining 60 % was used for network training and testing. This simulates two different sessions in a subject-centred network training scenario, first for hyperparameter optimization and then for training the optimal network. For both parameters, the tested values were 0.75, 0.8, 0.85, 0.9, 0.95 and 0.97, corresponding to time constants of 8.0, 10.3, 14.2, 21.9, 44.9, 75.6 ms. The results for the user-specific hyperparameter optimization, to find the combination of α and β that maximise the classification accuracy in the test phase, are shown in Figure 5. The results are provided for one representative subject, for the two layers of the network. Based on this grid search, we chose for each subject the best hyperparameter values, reported in Table 2. On average, across all layers, subjects, and α-β combinations, the accuracy was 0.95 ± 0.07.

2.3 Intra-user hand gesture classification

The optimised network was trained and tested for each subject by selecting different dataset portions of the remaining 60% of the dataset. The SNN training was run for 100 epochs, by grouping different classes, muscles and contraction phases. Figure 6 shows mean and standard deviation of test accuracy across subjects for each layer for three muscle groupings: all muscles (dark violet), intrinsic muscles (magenta), and extrinsic muscles (cyan), and for the three contraction phases. These values are reported both in the case of classifying 5

and 10 classes. We obtained an overall test accuracy of 0.92 ± 0.10 for all muscles, 0.83 ± 0.23 for only intrinsic and 0.86 ± 0.19 for only extrinsic, across all subjects, the two class selections (5 and 10), and the two layers respectively. The accuracy was 0.86 ± 0.20 for plateau (steady and isometric) contractions, while for increasing contractions (non-isometric) was 0.81 ± 0.20, and for both the contractions considered together was 0.95 ± 0.14.

The test accuracy performance of the second layer – across all subjects and the two class selections – was overall higher than for the first: 0.94 ± 0.1 (versus 0.91 ± 0.11) for all muscles, 0.91 ± 0.13 (versus 0.75 ± 0.28) for intrinsic, and 0.91 ± 0.14 (versus 0.81 ± 0.22) for extrinsic, with overall lower standard deviation in all cases. This applies also when analysing the different phases (I, P, I+P) of the movement: respectively the second versus the first layer presented an accuracy of 1.0 ± 0 versus 0.9 ± 0.18 for I+P, 0.86 ± 0.15 vs 0.75 ± 0.22 for I, and 0.9 ± 0.12 vs 0.82 ± 0.25 for P. Adding further layers did not improve these figures of merit, we therefore optimised the accuracy/resources trade-off using only two layers, in order to apply this structure for on-chip implementation. Sec. 2.6 presents the optimisation of computational resources, by analysing the test accuracy when progressively reducing the number of neurons.

2.4 Inter-subject hand gesture classification

In different recording sessions and for different subjects, the number of identified neurons by HD-sEMG decomposition is highly variable. This is because motor neuron identification is based on identifying the action potential waveforms of the most superficial motor units discriminable in the measured HD-sEMG signals. These waveforms depend on the conduction volume, which varies due to electrode displacement across different subjects and sessions. To have the same number of motor neurons per muscle for all the subjects, we selected a subset of the most active motor neurons (ordered by the number of spikes in each muscle) in a number equal to the minimum number of motor neurons identified for each muscle across the 5 subjects, reported in Table 1 (10, 3, 5, 4, 7, 0, 0, 3, 4, 5, 0, 6, 10, 0). From the dataset different portions were considered, i.e. the conditions of 5 classes and 10 classes, and all phases I+P, I and P, with a window width of 200 ms with no overlap. We chose a value of α and β as those corresponding to the best average across all subjects of the results obtained for each subject in the phase of hyperparameter optimization, corresponding to 0.97 for α and 0.75 for β. The overall test accuracy for the inter-subject dataset is of 0.74 ± 0.05 for all muscles, 0.64 ± 0.09 for intrinsic and 0.54 ± 0.05 for extrinsic (across layers and contraction phases). For the different movement phases, the accuracy was 0.7 ± 0.11 for P, 0.59 ± 0.09 for I and 0.62 ± 0.08 for I+P (across layers and muscle combinations). These values are on average lower than the mean values obtained for the intra-user classification.

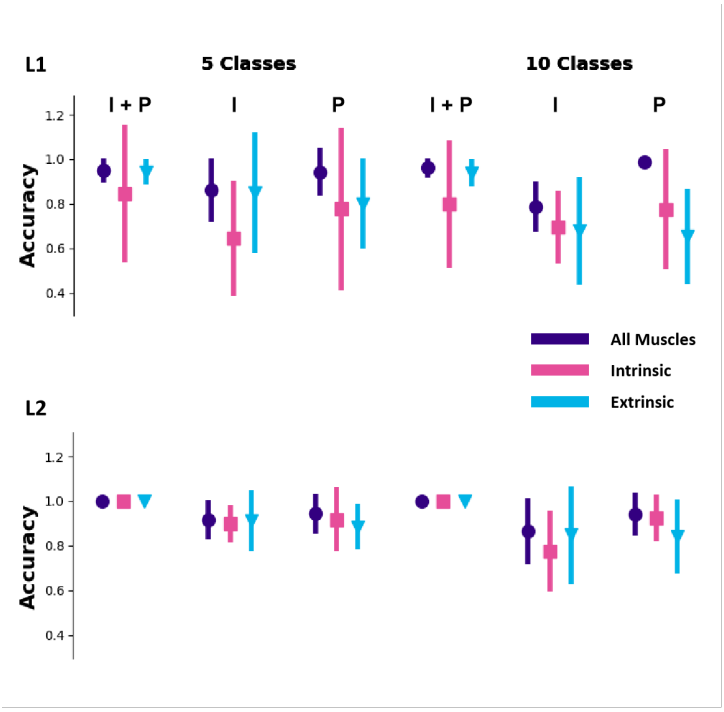

Fig. 6 Intra-user hand gesture classification. Mean and standard deviation for the test accuracy of the Spiking Neural Network (SNN), for layer 1 (L1) and layer 2 (L2), by grouping muscles in three different ways: all (dark violet), intrinsic (magenta), extrinsic (cyan), and by selecting three different periods of contraction: increasing plus plateau (I+P), increasing (I) and plateau (P). Each network is trained individually for each subject, test accuracy values are averaged across subjects.

2.5 Power Consumption

To compute the energy consumption and inference time of the convolutional SNN, we deployed the network onto the NVIDIA Jetson Nano, an embedded system with a 128-Core Maxwell GPU with 4GB 64-bit LPDDR4 memory 25.6 GB/s[1]. The energy consumption performance is presented as Energy-Delay Product (EDP), a metric suitable for most modern processor platforms, defined as the average energy consumption multiplied by the average inference time. The inference time is defined as the time elapsed between the end of the presented sample and the classification. The EDP was calculated using the dynamic power consumption, measured as the difference of total power consumed by the network and the static power, when the GPU is idle, that corresponds to 50 mW. The performance of the network was 100 mW (dynamic power) for a total consumed energy of 0.97 mJ and inference time of 9.7 ms, resulting in EDP at 9.4 uJ*s.

[1] https://developer.nvidia.com/embedded/jetson-nano-developer-kit

2.6 Optimisation of the network structure for minimising computational resources

The network architecture and hyperparameters used in the analysis above were selected empirically after testing different number of layers and number of neurons per layer. To test the trade-off between network size and accuracy, we implemented a single layer convolutional network and a single layer fully connected network. In both cases, the input size was equal to the number of motor neurons and the output size, respectively equal to 128, 64, 32, 16. The readout layer had an output equal to the number of classes to discriminate. We trained and tested these networks for all the subjects separately (intra-user), for all the 10 classes, only for the plateau phase, and for all muscles.

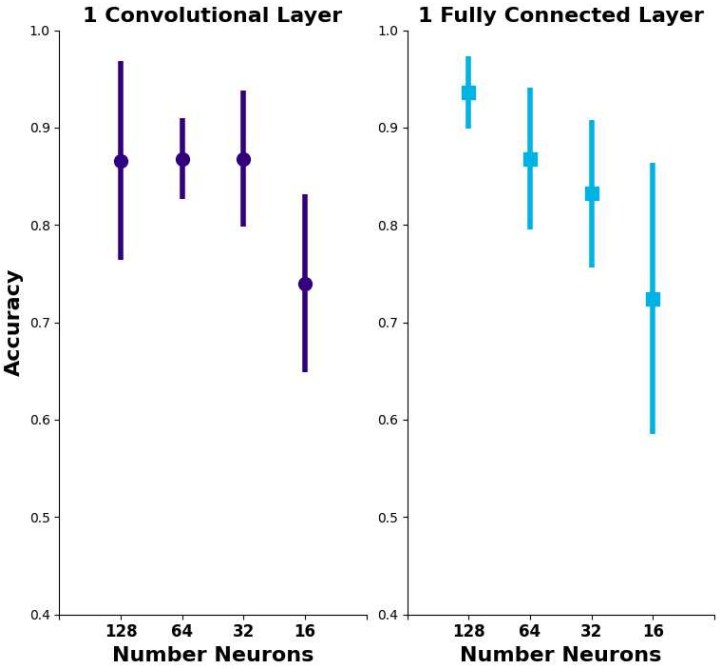

Fig. 7 Minimisation of computational resources. Mean and standard deviation across subjects of the test accuracy for the different network layers (convolutional or fully connected) by testing 4 different sizes, 128, 64, 32, and 16 neurons in the hidden layer (the input size was equal to the number of motor neurons to classify and the output equal to the 10 classes).

Figure 7 shows mean and standard deviation of the test accuracy across subjects, for varying the size of the single layer networks. While for the fully connected network we found a progressive decrease in accuracy by decreasing the size, for the convolutional network we found the same test accuracy for a size greater than or equal to 32 neurons, on average over 0.8 and similar to the value obtained with the fully connected layer with 64 neurons.

3 Discussions

We propose a neuromorphic framework for processing the spiking activity of human motor neurons, towards the design of wearable neural interfaces. Motor neuron activity was recorded in-vivo, during the execution of natural hand gestures. Movement intention was inferred from the spike trains of almost one hundred motor neurons for each subject (thus almost 500 motor neuron spike trains were processed in total). The spatio-temporal behaviour of the motor neurons was processed by artificial spiking LIF neurons. This framework unleashes the full potential of interfacing biological neurons with artificial spiking neurons, solely using spike-based encoding. The use of LIF neurons and local spike-driven plasticity rules opens up the possibility of implementing such architecture on neuromorphic chips, leading to an even more efficient online and wearable implementation. We considered muscles in the forearm (extrinsic), to target the use of myoelectric armbands and bracelets for monitoring users' activity [37, 38], and in the hand (intrinsic), so far considered mainly in neurophysiology [36, 39, 40].

We here processed an unprecedentedly complex dataset, involving 384 HD-sEMG channels targeting 14 hand muscles, and including gestures like single-finger flexion (5 classes), thumb movements and three different grip types (for a total of 10 classes), to include more natural gestures. This dataset also contains non-isometric contractions, implying an increasing of the contraction to perform one of the 10 gestures, followed by a plateau isometric phase for each gesture. We processed these contraction phases both separately and together, to understand during which phase of the motion the network can extract more information about the hand gesture. We studied the network performance when trained separately for each subject and when trained for all subjects, to validate its use in a user-centred approach whereby a pre-trained network can be adapted to a single user for best performance.

When using optimised hyperparameters to train the network with data of each individual user, we got a high accuracy of 0.95 ± 0.14 (across subjects and layers) considering all the muscles and both isometric and non-isometric contractions in the same training. When considering only the second layer the same combination (all muscles, all phases) led to an average accuracy of 1. This is an important result, enabling high classification accuracy of daily-life gestures, which can be non-isometric or pseudo-isometric in a variable way. Moreover, although the mean values across subjects were higher, no statistically significant difference was found in classification accuracy for different muscle groupings or contraction modes. This is another important outcome, meaning an invariant use of either myoelectric gloves or armband, according to the specific needs of the user, without significant loss of classification accuracy. In particular, at the second layer of the network we found less difference in classification accuracy among the three muscle groupings and an average higher classification performance. This means that adding a second layer can increase and stabilise the pattern recognition of neural spiking information encoding different gestures. Finally, we showed how to optimise the network

with a different combination of hyperparameters representing the neuron and the synapse time constants (respectively α and β). After an initial tuning, which could be performed by the user as a calibration phase to update periodically, the network can be fine-tuned with data from the user through local learning at each layer.

We also investigated the case of recognizing neural spiking patterns from a dataset containing information collected from many users, to create a general model of human neural patterns associated to gestures. This raises the problem of variability in number of identified motor neurons across different subjects, as shown in Table 1. In fact, the identification of motor unit action potentials associated to a single motor unit (thus a motor neuron) depends on the specific volume conduction of a certain session (position of the electrodes with respect to the muscles) and even more from the anatomic aspects of one subject (interposed tissues between electrodes and muscles, shape of the muscles and body metric). This could hinder the successful deployment of the system in myoelectric control whether the network would need to be trained on multiple subjects. Although it is reasonable for many applications to train the network specifically for one subject, leading to high accuracy as shown, developing universal models of human neural patterns could be useful for instance to avoid to train the model to each specific user, saving time during the usage. The solution that we proposed consists in extracting subsets of an equal number of motor neurons for each muscle for all the subjects and for all sessions, by selecting the most active motor neurons from each subject. However, we observe lower classification accuracy in this case, than when classifying patterns separately for each user. Further options in this direction could be the implementation of a customised input layer that adapts to the number of identified motor neurons with an arbitrary number of outputs, concatenated with the following layers trained on many subjects. Also, a training on a larger population of users and mapping more conditions and gestures would be necessary for a inter-user classification model of human motor intentions from motor neurons spiking activity.

To minimise the energy consumption and the time of computation needed for edge computing on wearable devices, the first requirement is minimizing the network size and number of operations (number of connections, neurons, layers, etc.), while maintaining reasonable levels of accuracy. For the shown results, we used 64 neurons and 128 neurons for the two convolutional layers, respectively, that leads to tens of thousands of synaptic connections (for a convolutional kernel size of 3). We observed that both for a convolutional and a fully connected layer with at least 32 neurons the test accuracy can be kept averagely over 0.8, although the convolutional layer shows slightly more stable performance by decreasing the number of neurons between 128 and 32.

Few examples of SNN processing biological neural information can be found in the literature. A first common approach is an artificial spike encoding of in-vivo neural biopotentials, like EEG and EMG. This spike encoding of the recorded signal is performed by thresholding the signal values exceeding a

baseline, with an asynchronous delta modulator approach [24, 25, 41]. Differently, in this study, we did not use an artificial spike encoding to extract spiking information from biopotentials, i.e. EMG, but we identified the natural spike encoding received by each single motor neuron from spinal neuronal circtuitries or super-spinal structures [42]. This spiking neural information is inherent in the recorded EMG signals and coupled with volume conduction information [43]. Through decomposition, we decoupled this neural spiking information from the conduction volume information (motor unit action potential waveforms). Thus, we did not feed a SNN with an artificial spike encoding from biopotentials, but with the true natural neural activity of human in-vivo neurons, e.g. spinal motor neurons. A second approach for SNN processing of biological neural information is processing in-vitro spiking information from a population of neurons plated onto a substrate-integrated multi electrode array [29–31] by recording from in-vitro neurons obtained from rat neocortex. Finally, a third approach is to record neuronal spikes from anesthetized animals while stimulating the nervous tissues to be processed with neuromorphic devices [32]. However, so far nobody attempted to process the activity of in-vivo human individual neurons receiving their spiking information from the CNS, i.e spinal and superspinal structures, during daily-life gesture execution [44].

This framework has been developed with the goal of implementation on neuromorphic chips, to minimise the energy footprint of the final neural interface. To this aim, technological aspects to map this architecture on neuromorphic chips need to be solved. Depending on the neuromorphic technology of choice, limitations due to the number of possible synaptic connections per neuron, limited weight resolution, and the implementation feasibility of specific learning rules need to be taken into account.

Thus, we propose this framework to be used in the next generation of neural interfaces with a broad range of purposes. Although we here accessed motor neuron spiking information via a non-invasive neural interface using blind source separation, motor neuron activity could be as well extracted using implantable devices targeting to nerves or the cortex. This would open the scenario of extending biological neuronal circuitry with artificial silicon neurons. This spiking neural information would lead to highly efficient processing and learning from network running either on GPU-clusters in cloud platforms or locally in a neuromorphic chip, opening new frontiers for product and services for communicating, gaming and health monitoring.

4 Methods

4.1 Subjects

Five healthy individuals (age: 27.2 ± 3.3 yrs; weight: 74.6 ± 7.1 kg; height: 179 ± 6.7 cm) participated in the experiments after having signed an informed consent form approved by the Imperial College London Research Ethics

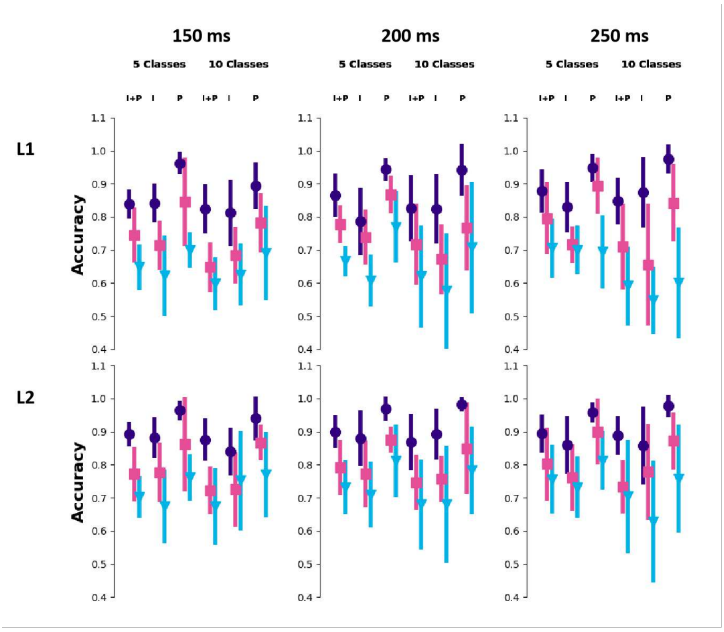

Fig. 8 Intra-user hand gesture classification across different windowing interval of the dataset, respectively 150, 200, and 250 ms. Mean and standard deviation for the test accuracy of the Spiking Neural Network (SNN), are reported as in Figure 6 for layers, muscle grouping, number of classes and contraction phase selection.

Committee (approval no. 18IC4685), in conformity with the Declaration of Helsinki.

4.2 Targeted muscles and gestures

The electrode configuration of the HD-sEMG represented in Figure 3.b maps the activity of 14 of the most important muscles actuating the finger and the wrist [36]. The recorded muscles were first dorsal interosseous (FDI), the three other dorsal interossei (II-IV DI), abductor digiti minimi (ADM), flexor pollicis brevis (FPB), abductor pollicis brevis (APB), opponens pollicis (OPP), extensor carpi ulnaris (ECU), extensor digitorum communis (EDC), extensor carpi radialis (ECR), flexor carpi ulnaris (FCU), flexor digitorum superficialis (FDS) and flexor carpi radialis (FCR).

Each subject performed 10 natural gestures (Fig. 3.a) of different complexity, comprising: flexion of each single finger, with the wrist respectively in neutral, extended and flexed position (15 recordings overall); abduction and opposition of the thumb, with the wrist in a neutral position; grips involving two, three and five fingers.

Each gesture lasted 6 seconds, for 4 repetitions. A pause of 1 minute between each recording of the 4 repetitions per gesture was interposed, to avoid the presence of fatigue effects. These 6 s were divided in 2 s for reaching the required finger posture (with an excursion of the interested joint angle

resulting in an increasing in the contraction), 2 s to block the finger posture (isometric part, with a plateau in the contraction), and 2 s to come back to the neutral position.

4.3 Experimental Setup

Six 64-channel grids with equidistant electrodes covered the forearm and the hand: two grids (8 mm inter-electrode distance (IED)) over the extrinsic (into the forearm) extensor and flexor muscles, four grids (4 mm IED) over the intrinsic muscles (into the hand). HD-sEMG signals were recorded with a monopolar recording configuration by a 400-channels amplifier (Quattrocento, OT Bioelettronica, Torino, Italy). Signals were amplified with a gain of 150, band-pass filtered between 10 and 900 Hz, sampled at 2048 Hz, and A/D converted to 16 bits. A laptop received the digitised data to store and visualise it in real-time. A monitor was placed in front of each participant to represent a picture indicating the gesture to execute and the timings of the execution. This visual feedback was represented with a custom-made application developed in Matlab (The Mathworks, Natick, US), which also visualised and saved the HD-sEMG signals.

4.4 Signal Processing

Convolution Kernel Compensation (CKC) is a blind source separation method to separate the electrical activity of the motor units concurrently activated during the recording. Each HD-sEMG signal is a different observation of the mixture of the motor unit electrical activity. Each motor unit is characterised by a different motor unit action potential waveform depending on the properties of the conduction volume [34]. The decomposition exploits CKC to distinguish similar motor unit action potential waveforms. Similar action potential waveforms across the HD-sEMG electrodes are recognised as firing occurrences of the same motor unit (Fig. 2.b).

To identify the motor neurons firing patterns of the investigated muscles and track the same motor neurons across multiple tasks, we concatenated the HD-sEMG signals of the recordings relative to each gesture and then decomposed the concatenated HD-sEMG as in [40]. Each group of 64 concatenated HD-sEMG signals corresponding to a recording grid of 64 electrodes was decomposed separately with the CKC algorithm [45] (Fig. 2). Since the amount of HD-sEMG data to decompose for all the gestures exceeded the computational capacity of the decomposition algorithm, HD-sEMG data were divided in 4 different concatenations. The order of concatenation of the HD-sEMG recordings was:

- **Grips**: Five-finger grips, Three-finger grip, Two-finger grip
- **Neutral wrist**: Index, Little, Middle, Ring, Thumb flexion, Thumb Abduction, Thumb Opposition
- **Extended wrist**: Index, Little, Middle, Ring, Thumb flexion
- **Flexed wrist**: Index, Little, Middle, Ring, Thumb flexion

The concatenated HD-sEMG signals were digitally filtered between 20 and 500 Hz with a 4th-order Butterworth filter and then decomposed by the CKC algorithm [45]. The accuracy of this motor unit identification from HD-sEMG was assessed by PNR [35]. The final output of the decomposition was manually inspected by expert operators [46].

To complete the motor neuron tracking across all the observed recordings, after having decomposed separately the four HD-sEMG concatenations, the spiking activity of the identified spinal motor neurons for each concatenation was matched across all the other concatenations. To do so, we paired similar action potential waveforms of the respective motor units across the four concatenations, by ordering similar motor unit pairings from the most similar to the least similar until the termination of the pairings. Waveform similarity was assessed with a 2D-cross-correlation between the matched motor unit action potential templates. The average action potential waveforms for each electrode were obtained by spike-triggered average (STA) [47]. We included in the analysis all the identified motor neurons, also the ones which were not tracked across two different concatenations by STA, as explained above.

Each motor neuron was then associated to a muscle, with a process consisting of four steps: a) finding the motor unit location by quantifying the amplitude distribution of the action potential waveforms for each electrode obtained by STA, b) dividing arbitrarily the grid covering more than one muscle in three transverse bands with respect to the grid longer axis, c) computing the mean root mean square (RMS) value of the averaged waveforms of all the channels for each band, and d) taking the band among the three with the higher mean RMS value. This process is described in detail in [40]. Motor neurons were then ordered by muscle.

4.5 Choice of the processing window for the SNN

We present in the results the performance of the SNN with a dataset of motor neuron activity windowed at 200 ms. Although this is a commonly accepted window width for myoelectric control, other intervals could be chosen under 300 ms [48]. Thus, we previously tested the case of 150, 200 and 250 ms as presented in Figure 8, to conclude that there was not any statistic significance in the use of these three windows, all respecting the requirement for myoelectric control prescribed in the literature. Values- of test accuracy of the central column, corresponding to 200 ms of processing window, are not comparable with the ones of Figure 6, using the same window width, because the network was run on different portion of the datasets and with different hyperparameters, since it was a preliminary test to evaluate the processing window.

4.6 Hyperparameters optimization and simulation of different recording condition: intra-user analysis

The spiking activity of individual spinal motor neurons innervating the targeted muscles was directly interfaced with a convolutional SNN composed by

two layers of LIF neurons (Fig. 1). Each of the two convolutional layers was trained autonomously, by surrogate gradient and local learning. The network is mainly ruled by the time constant of the neurons' membrane, and of the synapses, represented by the α and β hyperparameters, respectively. α and β were tuned specifically for each subject during network training. Then, fixed the optimal hyperparameters, different recording conditions were simulated by considering different selections of muscles (only intrinsic, only extrinsic or both groups), classes (only single finger flexion or also thumb abduction, opposition and 3 different grips) and phases of contractions.

4.7 Inter-user classification

The same analysis was performed for inter-user classification, training a network with data of multiple subjects. The lack of data consistency due to the variability of the number of identified motor neurons across subjects is solved by taking the same subset of motor neurons for each muscle for all the subjects for creating a multi-subject dataset.

5 Funding

For this study, DF was sponsored by the European Research Council (ERC) under the Synergy Grant Natural BionicS (810346) and the EPSRC Transformative Healthcare for 2050 project NISNEM Technology (EP/T020970/1).

References

[1] Navarro, X. *et al.* A critical review of interfaces with the peripheral nervous system for the control of neuroprostheses and hybrid bionic systems. *Journal of the Peripheral Nervous System* **10** (3), 229–258 (2005). https://doi.org/10.1111/j.1085-9489.2005.10303.x .

[2] Farina, D. *et al.* Toward higher-performance bionic limbs for wider clinical use. *Nature Biomedical Engineering* (2021). https://doi.org/10.1038/s41551-021-00732-x .

[3] Hargrove, L. J., Lock, B. A. & Simon, A. M. Pattern recognition control outperforms conventional myoelectric control in upper limb patients with targeted muscle reinnervation. *Proceedings of the Annual International Conference of the IEEE Engineering in Medicine and Biology Society, EMBS* 1599–1602 (2013). https://doi.org/10.1109/EMBC.2013.6609821 .

[4] Kamavuako, E. N., Scheme, E. J. & Englehart, K. B. Combined surface and intramuscular EMG for improved real-time myoelectric control performance. *Biomedical Signal Processing and Control* **10** (1), 102–107 (2014). URL http://dx.doi.org/10.1016/j.bspc.2014.01.007. https://doi.org/10.1016/j.bspc.2014.01.007 .

[5] Smith, L. H., Kuiken, T. A. & Hargrove, L. J. Linear regression using intramuscular EMG for simultaneous myoelectric control of a wrist and hand system. *International IEEE/EMBS Conference on Neural Engineering, NER* **2015-July**, 619–622 (2015). https://doi.org/10.1109/NER.2015.7146699 .

[6] Connan, M., Kõiva, R. & Castellini, C. Online Natural Myocontrol of Combined Hand and Wrist Actions Using Tactile Myography and the Biomechanics of Grasping. *Frontiers in Neurorobotics* **14** (February), 1–16 (2020). https://doi.org/10.3389/fnbot.2020.00011 .

[7] Farina, D. *et al.* Man/machine interface based on the discharge timings of spinal motor neurons after targeted muscle reinnervation. *Nature Biomedical Engineering* **1** (2), 1–12 (2017). https://doi.org/10.1038/s41551-016-0025 .

[8] Chen, C. *et al.* Prediction of finger kinematics from discharge timings of motor units: Implications for intuitive control of myoelectric prostheses. *Journal of Neural Engineering* **16** (2) (2019). https://doi.org/10.1088/1741-2552/aaf4c3 .

[9] Puttaraksa, G. *et al.* Voluntary and tremorogenic inputs to motor neuron pools of agonist/antagonist muscles in essential tremor patients. *Journal of Neurophysiology* **122** (5), 2043–2053 (2019). https://doi.org/10.1152/jn.00407.2019 .

[10] Gallego, J. A. *et al.* Influence of common synaptic input to motor neurons on the neural drive to muscle in essential tremor. *Journal of Neurophysiology* **113** (1), 182–191 (2015). https://doi.org/10.1152/jn.00531.2014 .

[11] Williams, S. E., Koch, K. C. & Disselhorst-Klug, C. Non-invasive assessment of motor unit activation in relation to motor neuron level and lesion location in stroke and spinal muscular atrophy. *Clinical Biomechanics* **78** (August 2019) (2020). https://doi.org/10.1016/j.clinbiomech.2020.105053 .

[12] Murphy, S. A. *et al.* Stroke increases ischemia-related decreases in motor unit discharge rates. *Journal of Neurophysiology* **120** (6), 3246–3256 (2018). https://doi.org/10.1152/jn.00923.2017 .

[13] Park, I. M., Seth, S., Paiva, A. R., Li, L. & Principe, J. C. Kernel methods on spike train space for neuroscience: A tutorial. *IEEE Signal Processing Magazine* **30** (4), 149–160 (2013). https://doi.org/10.1109/MSP.2013.2251072, https://arxiv.org/abs/1302.5964 .

[14] Kayser, C., Montemurro, M. A., Logothetis, N. K. & Panzeri, S. Spike-phase coding boosts and stabilizes information carried by spatial and temporal spike patterns. *Neuron* **61** (4), 597–608 (2009). URL https://www.sciencedirect.com/science/article/pii/S0896627309000750. https://doi.org/https://doi.org/10.1016/j.neuron.2009.01.008 .

[15] Panzeri, S., Ince, R. A., Diamond, M. E. & Kayser, C. Reading spike timing without a clock: intrinsic decoding of spike trains. *Philosophical Transactions of the Royal Society B: Biological Sciences* **369** (1637), 20120467 (2014) .

[16] Belitski, A., Panzeri, S., Magri, C., Logothetis, N. K. & Kayser, C. Sensory information in local field potentials and spikes from visual and auditory cortices: time scales and frequency bands. *Journal of Computational Neuroscience* **29** (3), 533–545 (2010). URL https://doi.org/10.1007/s10827-010-0230-y. https://doi.org/10.1007/s10827-010-0230-y .

[17] Pica, G. *et al. Quantifying how much sensory information in a neural code is relevant for behavior*, NIPS'17, 3689–3699 (Curran Associates Inc., Red Hook, NY, USA, 2017).

[18] Gerstner, W., Kistler, W. M., Naud, R. & Paninski, L. *Neuronal dynamics: From single neurons to networks and models of cognition* Cambridge edn. October 2013 (2014).

[19] Illing, B., Gerstner, W. & Brea, J. Biologically plausible deep learning — but how far can we go with shallow networks? *Neural Networks* **118**, 90–101 (2019). URL https://www.sciencedirect.com/science/article/pii/S0893608019301741. https://doi.org/https://doi.org/10.1016/j.neunet.2019.06.001 .

[20] Tavanaei, A., Ghodrati, M., Kheradpisheh, S. R. & Reza, S. Deep Learning in Spiking Neural Networks. *Neural Networks* **111**, 47–63 (2019). URL https://doi.org/10.1016/j.neunet.2018.12.002. https://doi.org/10.1016/j.neunet.2018.12.002, https://arxiv.org/abs/1804.08150v4 .

[21] Balaji, A. *et al.* Mapping spiking neural networks to neuromorphic hardware. *IEEE Transactions on Very Large Scale Integration (VLSI) Systems* **28** (1), 76–86 (2020). https://doi.org/10.1109/TVLSI.2019.2951493 .

[22] Chicca, E., Stefanini, F., Bartolozzi, C. & Indiveri, G. Neuromorphic electronic circuits for building autonomous cognitive systems. *Proceedings of the IEEE* **102** (9), 1367–1388 (2014) .

[23] Rajendran, B., Sebastian, A., Schmuker, M., Srinivasa, N. & Eleftheriou, E. Low-power neuromorphic hardware for signal processing applications:

A review of architectural and system-level design approaches. *IEEE Signal Processing Magazine* **36** (6), 97–110 (2019). https://doi.org/10.1109/MSP.2019.2933719 .

[24] Ma, Y. *et al.* Emg-based gestures classification using a mixed-signal neuromorphic processing system. *IEEE Journal on Emerging and Selected Topics in Circuits and Systems* **10** (4), 578–587 (2020) .

[25] Donati, E., Payvand, M., Risi, N., Krause, R. & Indiveri, G. Discrimination of EMG Signals Using a Neuromorphic Implementation of a Spiking Neural Network. *IEEE Transactions on Biomedical Circuits and Systems* **13** (5), 793–801 (2019). https://doi.org/10.1109/TBCAS.2019.2925454 .

[26] Bauer, F., Muir, D. & Indiveri, G. Real-time ultra-low power ECG anomaly detection using an event-driven neuromorphic processor. *Biomedical Circuits and Systems, IEEE Transactions on* **13** (6), 1575–1582 (2019). https://doi.org/10.1109/TBCAS.2019.2953001 .

[27] Das, A. *et al. Mapping of local and global synapses on spiking neuromorphic hardware*, 1217–1222 (IEEE, 2018).

[28] Ceolini, E. *et al.* Hand-gesture recognition based on emg and event-based camera sensor fusion: A benchmark in neuromorphic computing. *Frontiers in Neuroscience* **14**, 637 (2020) .

[29] Keren, H., Partzsch, J., Marom, S. & Mayr, C. G. A biohybrid setup for coupling biological and neuromorphic neural networks. *Frontiers in Neuroscience* **13** (MAY), 1–11 (2019). https://doi.org/10.3389/fnins.2019.00432 .

[30] Broccard, F. D., Joshi, S., Wang, J. & Cauwenberghs, G. Neuromorphic neural interfaces: From neurophysiological inspiration to biohybrid coupling with nervous systems. *Journal of Neural Engineering* **14** (4) (2017). https://doi.org/10.1088/1741-2552/aa67a9 .

[31] Buccelli, S. *et al.* A Neuromorphic Prosthesis to Restore Communication in Neuronal Networks A Neuromorphic Prosthesis to Restore Communication in Neuronal Networks. *iScience* 402–414 (2019). https://doi.org/10.1016/j.isci.2019.07.046 .

[32] Boi, F. *et al.* A bidirectional brain-machine interface featuring a neuromorphic hardware decoder. *Frontiers in Neuroscience* **10** (December), 1–15 (2016). https://doi.org/10.3389/fnins.2016.00563 .

[33] Kaiser, J., Mostafa, H. & Neftci, E. Synaptic Plasticity Dynamics for Deep Continuous Local Learning (DECOLLE). *Frontiers in Neuroscience* **14** (May), 1–11 (2020). https://doi.org/10.3389/fnins.2020.00424, https:

//arxiv.org/abs/1811.10766 .

[34] Farina, D., Merletti, R. & Enoka, R. M. The extraction of neural strategies from the surface EMG: An update. *Journal of Applied Physiology* **117** (11), 1215–1230 (2014). https://doi.org/10.1152/japplphysiol.00162.2014 .

[35] Holobar, A., Minetto, M. A. & Farina, D. Accurate identification of motor unit discharge patterns from high-density surface EMG and validation with a novel signal-based performance metric. *Journal of Neural Engineering* **11** (1) (2014). https://doi.org/10.1088/1741-2560/11/1/016008 .

[36] Tanzarella, S., Muceli, S., Del Vecchio, A., Casolo, A. & Farina, D. Non-invasive analysis of motor neurons controlling the intrinsic and extrinsic muscles of the hand. *Journal of Neural Engineering* **17** (4) (2020). https://doi.org/10.1088/1741-2552/aba6db .

[37] Gao, X. & Yin, Y. Design on a wearable armband device for assessing the motion function of upper limbs. *Computer Communications* **153** (February), 135–144 (2020). URL https://doi.org/10.1016/j.comcom.2020.01.074. https://doi.org/10.1016/j.comcom.2020.01.074 .

[38] Ruvalcaba, J. A., Gutiérrez, M. I., Vera, A. & Leija, L. Wearable Active Electrode for sEMG Monitoring Using Two-Channel Brass Dry Electrodes with Reduced Electronics. *Journal of Healthcare Engineering* **2020** (2020). https://doi.org/10.1155/2020/5950218 .

[39] Winges, S. A., Kornatz, K. W. & Santello, M. Common input to motor units of intrinsic and extrinsic hand muscles during two-digit object hold. *Journal of Neurophysiology* **99** (3), 1119–1126 (2008). https://doi.org/10.1152/jn.01059.2007 .

[40] Tanzarella, S., Muceli, S., Santello, M. & Farina, D. Synergistic Organization of neural inputs from spinal motor neurons to extrinsic and intrinsic hand muscles. *Journal of Neuroscience* (2021) .

[41] Corradi, F. & Indiveri, G. A Neuromorphic Event-Based Neural Recording System for Smart Brain-Machine-Interfaces. *IEEE Transactions on Biomedical Circuits and Systems* **9** (5), 699–709 (2015). https://doi.org/10.1109/TBCAS.2015.2479256 .

[42] Lemon, R. N. Descending pathways in motor control. *Annual Review of Neuroscience* **31** (Cm), 195–218 (2008). https://doi.org/10.1146/annurev.neuro.31.060407.125547 .

[43] Farina, D., Merletti, R. & Enoka, R. M. The extraction of neural strategies from the surface EMG (2004).

[44] Yoo, J. & Shoaran, M. Neural interface systems with on-device computing: machine learning and neuromorphic architectures. *Current Opinion in Biotechnology* **72** (Ml), 95–101 (2021). URL https://doi.org/10.1016/j.copbio.2021.10.012. https://doi.org/10.1016/j.copbio.2021.10.012 .

[45] Holobar, A. & Zazula, D. Multichannel blind source separation using convolution Kernel compensation. *IEEE Transactions on Signal Processing* **55** (9), 4487–4496 (2007). https://doi.org/10.1109/TSP.2007.896108 .

[46] Del Vecchio, A. *et al.* The human central nervous system transmits common synaptic inputs to distinct motor neuron pools during non-synergistic digit actions. *Journal of Physiology* **597** (24), 5935–5948 (2019). https://doi.org/10.1113/JP278623 .

[47] Martinez-Valdes, E. *et al.* Tracking motor units longitudinally across experimental sessions with high-density surface electromyography. *Journal of Physiology* **595** (5), 1479–1496 (2017). https://doi.org/10.1113/JP273662 .

[48] Phinyomark, A. *et al.* EMG feature evaluation for improving myoelectric pattern recognition robustness. *Expert Systems with Applications* **40** (12), 4832–4840 (2013). URL http://dx.doi.org/10.1016/j.eswa.2013.02.023. https://doi.org/10.1016/j.eswa.2013.02.023 .

Figures

Figure 1

Non-invasive neural interfaces for neuromorphic implementation. Human spinal motor neurons spike trains, inferred from surface electromyography (sEMG), are interfaced with an artificial Spiking Neural Network (SNN) of Leaky Integrate-and-Fire (LIF) neurons with local learning rules. The input to motor neurons is the net output of the integration performed by spinal interneurons of supraspinal and afferent neurons, encoded in the spiking activity of the motor neuron. The SNN main hyperparameters are α and β, the neuron's membrane and synaptic time constants, respectively.

Figure 2

Signal processing and motor neuron identification. a) High-Density-sEMG (HD-sEMG) recordings, concatenated across tasks, are decomposed in the corresponding trains of motor unit action potentials, to obtain the relative motor neuron spike trains tracked across different tasks. b) Identification of 2 motor units by HD-sEMG decomposition: the decomposition exploits blind source separation to distinguish similar motor unit action potential waveforms. c) The identified spike trains for one task are segmented in 200 ms-width windows and used as inputs to the convolutional Spiking Neural Network (SNN).

Figure 3

Experimental protocol and High-Density-sEMG (HD-sEMG) electrode placement. a) The protocol included single-finger flexion (5 gestures), 3 different grips with 5, 3 and 2 fingers, and thumb abduction and opposition (10 gestures in total). b) 6 HD-sEMG grids each with 64-channels recorded the activity of 14 muscles. Two large grids (8mm Intra□Electrode Distance (IED)) were placed over the forearm and four small grids were placed over intrinsic muscles (4mm IED).

Figure 4

Structure of the convolutional Spiking Neural Network (SNN) adopted in the study. The overall structure of the network comprises two convolutional spiking layers (Conv), and two pool layers (Pool). Two fully connected (FC) layers are appended each one at the end of each Conv-Pool structure, to implement the local learning. The dimension of their output is the number of classes. The number of neurons (N) in the

input layer corresponds to the number of motor neurons identified for each subject, varying for each subject, as reported in Table 1.

Figure 5

Grid search for the optimisation of the hyperparameters α and β, respectively related to the membrane and synaptic constants. Mean and standard deviation across subjects and network layers of the maximal test accuracy across 100 epochs of training are reported, normalised between 0 and 1.

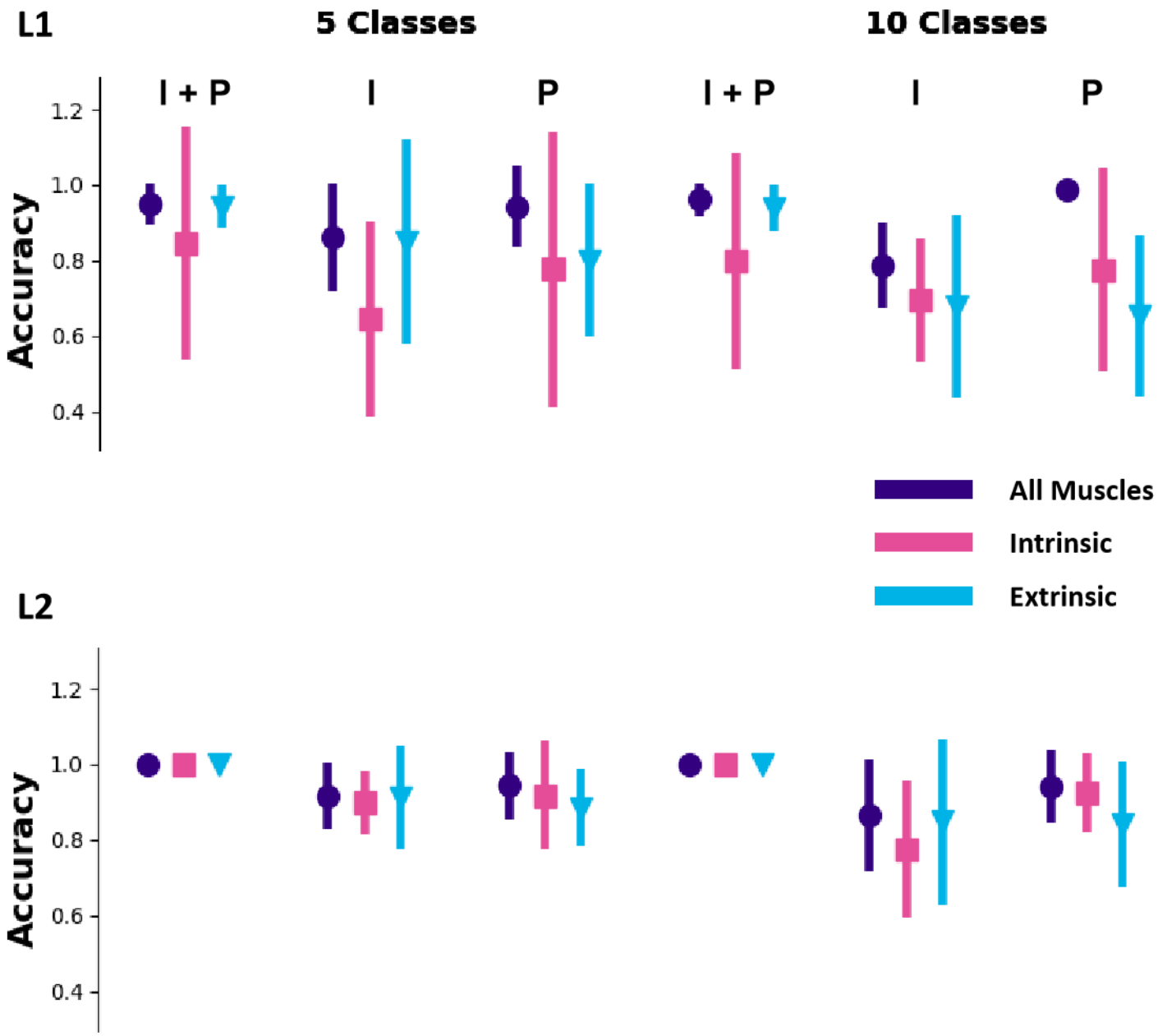

Figure 6

Intra-user hand gesture classification. Mean and standard deviation for the test accuracy of the Spiking Neural Network (SNN), for layer 1 (L1) and layer 2 (L2), by grouping muscles in three different ways: all (dark violet), intrinsic (magenta), extrinsic (cyan), and by selecting three different periods of contraction: increasing plus plateau (I+P), increasing (I) and plateau (P). Each network is trained individually for each subject, test accuracy values are averaged across subjects.

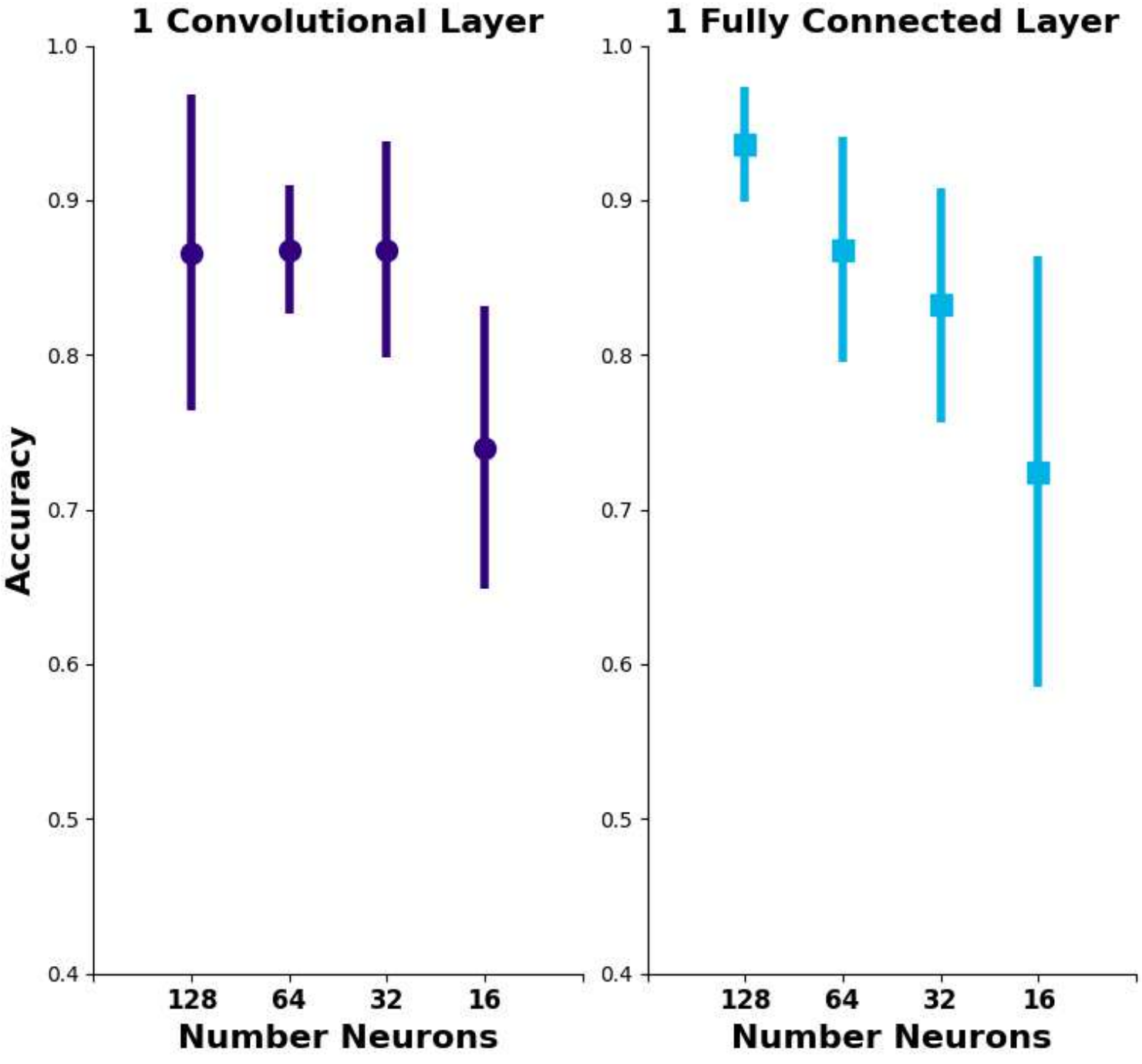

Figure 7

Minimisation of computational resources. Mean and standard deviation across sub□jects of the test accuracy for the different network layers (convolutional or fully connected) by testing 4 different sizes, 128, 64, 32, and 16 neurons in the hidden layer (the input size was equal to the number of motor neurons to classify and the output equal to the 10 classes).

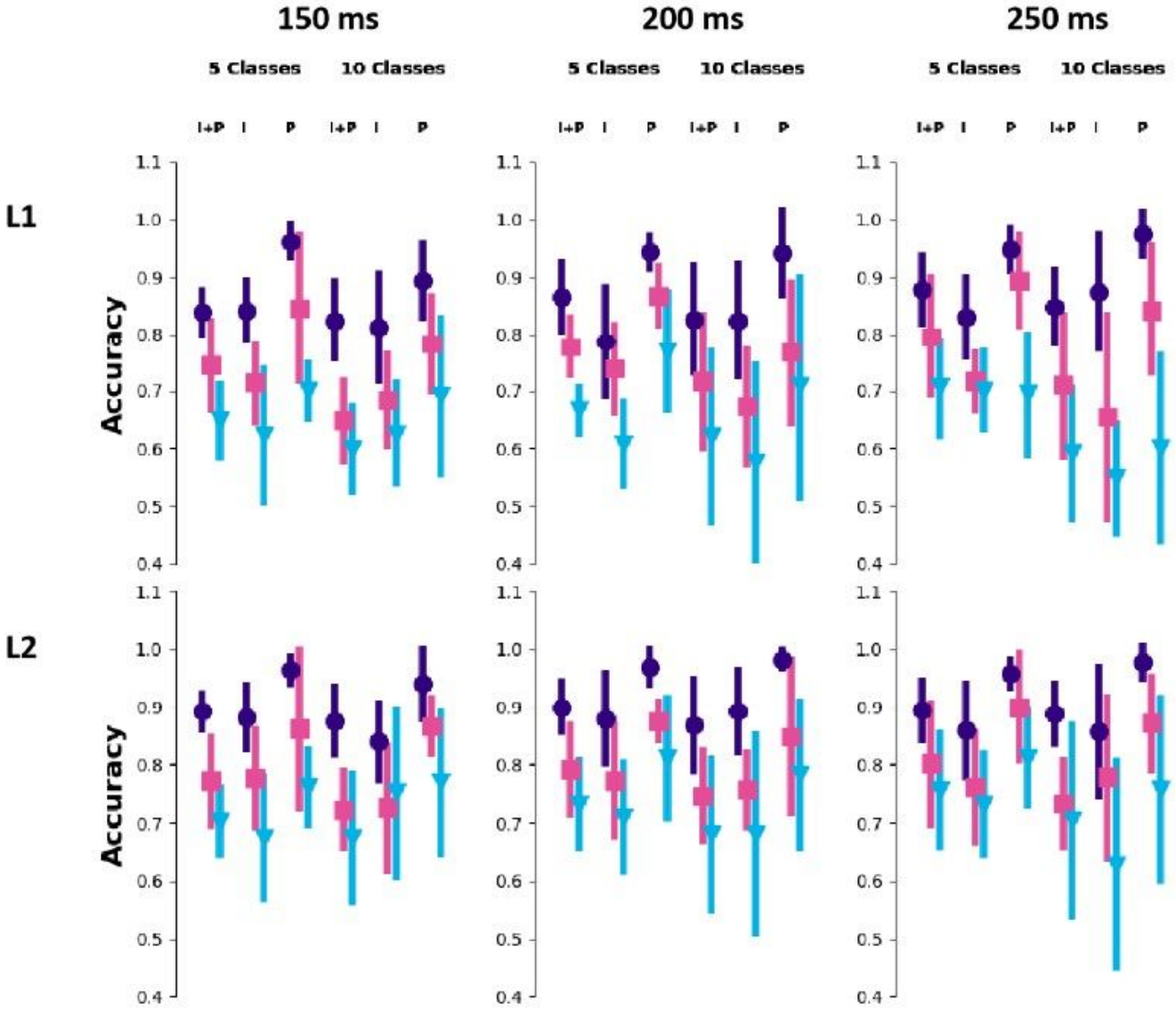

Figure 8

Intra-user hand gesture classification across different windowing interval of the

dataset, respectively 150, 200, and 250 ms. Mean and standard deviation for the test accuracy of the Spiking Neural Network (SNN), are reported as in Figure 6 for layers, muscle grouping, number of classes and contraction phase selection.